

A Comparative Study on the Cutting Performance of Uncoated, AlTiN and TiCN-Al₂O₃ Coated Carbide Inserts in Turning of Invar 36 Alloy

Mahir Akgün

Aksaray University, Technical Sciences Vocational School, Machine and Metal Technology, Aksaray, Turkey

Accepted 9 May 2022

Abstract

The present work focuses on a comparison of the performance of, a two-layer (TiCN-Al₂O₃) coated, the single-layer (AlTiN), and uncoated inserts in the machining of Invar 36, which is a difficult material to cut. The cutting performance of these tools has been appraised regarding cutting force (Fc), surface roughness (Ra), tool wear (Vb), and power consumption (Pc). Statistical analyzes were applied to determine the sustainable processing parameters of Invar 36. The outcomes of this study show that the two-layer (TiCN-Al₂O₃) coated insert performs a significant exhibiting in improving the cutting performance of Invar 36 alloy comparison with uncoated and single-layer (AlTiN) coated inserts. The tool wear is about 30% and 60% better using the two-layer (TiCN-Al₂O₃) coated insert than the single-layer (AlTiN) coated and uncoated inserts, respectively. The statistical analysis results, on the other hand, show that the ideal level groups for the lowest Fc, Ra, Vb, and Pc were A3B3C1, A3B3C1, A3B1C1, and A3B1C1, respectively. Moreover, the models developed to estimate the output parameters (Fc, Ra, Vb, and Pc) give successful results with high coefficients of determination (R²) of 93.18%, 98.79%, 98.05%, and 98.11%, respectively.

1. Introduction

Although the world's traditional energy resources are limited, energy demand is increasing day by day as a result of the continuous increase in population and industrialization. Nowadays, the increasing use of fossil energy sources causes many destructive effects on the environment at the global level [1]. Therefore, Sustainability requirements need to be met in all economic activities, especially in the industrial sector [2]. The basic principle of the concept of sustainability can be expressed as increasing the quality of life reducing environmental impacts using renewable resources [3]. In metal cutting industry, this concept is achieved by improving environmental friendliness, reducing waste, reducing energy consumption, and enhances occupational and worker health. For example, cutting fluids used in manufacturing industries, more than half of the oils used worldwide are petroleum-based, and they have negative effects on the environment and human health due to their disadvantages such as high post-process disposal costs, being toxic, and non-biodegradable [4]. On the other hand, cutting conditions in metalworking industry are often chosen based on an operator's

experience or practical knowledge. [5]. Nevertheless, it isn't easy to attain a sustainable process in this way. In the last decade, it has been observed that the application of innovative and environmentally friendly cooling/lubrication systems and optimization methods has increased to overcome these situations [6-9].

Invar 36 (Fe-36Ni), developed by Charles-Édouard Guillaume, is a binary Iron-Nickel alloy containing 36% nickel. The main feature of this alloy is its extremely low thermal expansion coefficient at room temperature, providing dimensional stability for all kinds of applications. The name of Invar comes from the word invariant, referring to this property, i.e., the "invariance of dimensions" [10-13]. Moreover, under the Curie temperature (279°C) conditions, the Invar 36 alloy is ferromagnetic and offers an extremely low thermal expansion coefficient. By taking advantage of this remarkable dimensional invariance over a wide operating temperature range, Invar 36 alloy is preferred in engineering applications where high dimensional stability is required under severe

temperature changes [14]. In particular, it is widely used in the aerospace industry components such as space cameras, precision instruments, ring laser gyroscopes, optical assembly components, twin metallic markers, seismic creep sensors, timekeeping instruments, and many applications such as metrology devices and television shadow-mask frames [15-17]. Recently, it has been focused on the production of many components with this material by additive manufacturing methods.

Invar 36 alloy consists of a single-phase austenite (γ -Fe) with a face-centered cubic (FCC) crystal structure. The high ductility, low thermal conductivity, and excessive work hardening tendency of austenitic alloys are considered reasons for their arduous machining [18, 19]. These properties often cause high cutting forces and high cutting temperature, and high abrasive wear of cutting tools due to the formation of hard carbides depending quick strain hardening during machining [20]. Moreover, built-up edge (BUE) formation in the machining process of Invar 36 severely affects cutting tool life, surface finish and production efficiency [21]. For these reasons, it is very important to define the ideal machining terms in terms of surface quality, cutting forces, tool life, and energy consumption, which are essential machinability criteria for a sustainable machining process concerning time and production efficiency.

Coated cutting tools are widely used in the metal cutting industry as they provide longer tool life, better predictability, and improved safety. Generally, cutting tools are coated using two different methods: physical vapor deposition (PVD) and chemical vapor deposition (CVD) [22]. In recent years, there are numerous studies evaluating the mechanism of tool wear, tool life, and machining performance of PVD and CVD coatings during machining of nickel-based superalloys. For example, Ezugwu and Okeke investigated the influences of the cutting tool coating on tool life, F_c and R_a in the turning of Nimonic C-263 alloy and found that TiN/TiCN/TiN coated inserts are better than TiAlN, coated inserts in terms of tool life, F_c , and R_a [23]. Then, in their other work, they investigated the influences of the cutting tool coating on tool life and surface integrity [24]. It has been observed that the multilayer PVD-TiN/TiCN/TiN coated gave the best performance, compared to PVD-TiN and CVD-TiC/Al₂O₃/TiN coated carbide tools in terms of tool life. Moreover, Jawadi et al. were compared the performance of PVD-TiN and CVD-TiCN+Al₂O₃ cutting tools in face milling of Inconel 718 superalloy [25]. The results showed that the CVD coated tool outperformed the PVD coated tool. They

attributed this to the slightly rounded edges of the CVD tool before the coating process.

From the above-mentioned literature survey, it can be stated that the cutting performances of various tools coated with PVD, and CVD methods are compared in terms of tool life, tool wear, surface integrity, and cutting forces in the machining of difficult-to-cut materials. However, there is very limited work on the machining of Invar 36 alloy, which is one of the hard-to-cut materials while there are studies on the production with mostly additive manufacturing methods. In this proposed study, the main difference is to examine the cutting performance of uncoated, CVD and PVD coated cutting tools in the machining of Invar 36 alloy, which is one of the hard-to-cut materials, and to define the ideal cutting parameters in terms of R_a , F_c , V_b and especially P_c . There are primary contributions of this work are illustrated as;

- To evaluate the performance of the cutting tool coating type in turning of the aerospace alloy.
- To perform a comprehensive investigation to observe the impacts of machining parameters on machining of Invar 36 alloy.
- Investigating the wear mechanism of the inserts with SEM.
- Determining the ideal process parameters in terms of R_a , F_c , V_b , and especially P_c with the Taguchi method.

2. Experimental

2.1 Turning Experiments and Cutting Tool

The machining tests have been performed out on CNC lathe without coolant. The spindle motor power of the machine was 15 KW, and the spindle with stepless variable speed could reach 3500 rpm maximum speed. The workpiece specimens 200 mm long and 25.4 mm in diameter. In these tests, the uncoated, single-layer (AlTiN) coated, and two-layer (TiCN-Al₂O₃) coated cutting tools were used. These cutting tools were commercial-grade inserts manufactured by Kennametal with the geometry of CNMG. Moreover, the uncoated, AlTiN coated and TiCN-Al₂O₃ coated carbide tools which have K68, KC5010, and KCM15 grade in ISO, respectively have attached on the tool holder (PCLNR 2525M-12 tool holder). The manufacturer's recommendations and previous studies on superalloys were considered in selecting cutting tools and determining the cutting parameter levels. Turning parameters and levels are given in Table 1. SEM images of the microstructure of the carbide inserts are seen in Fig. 1.

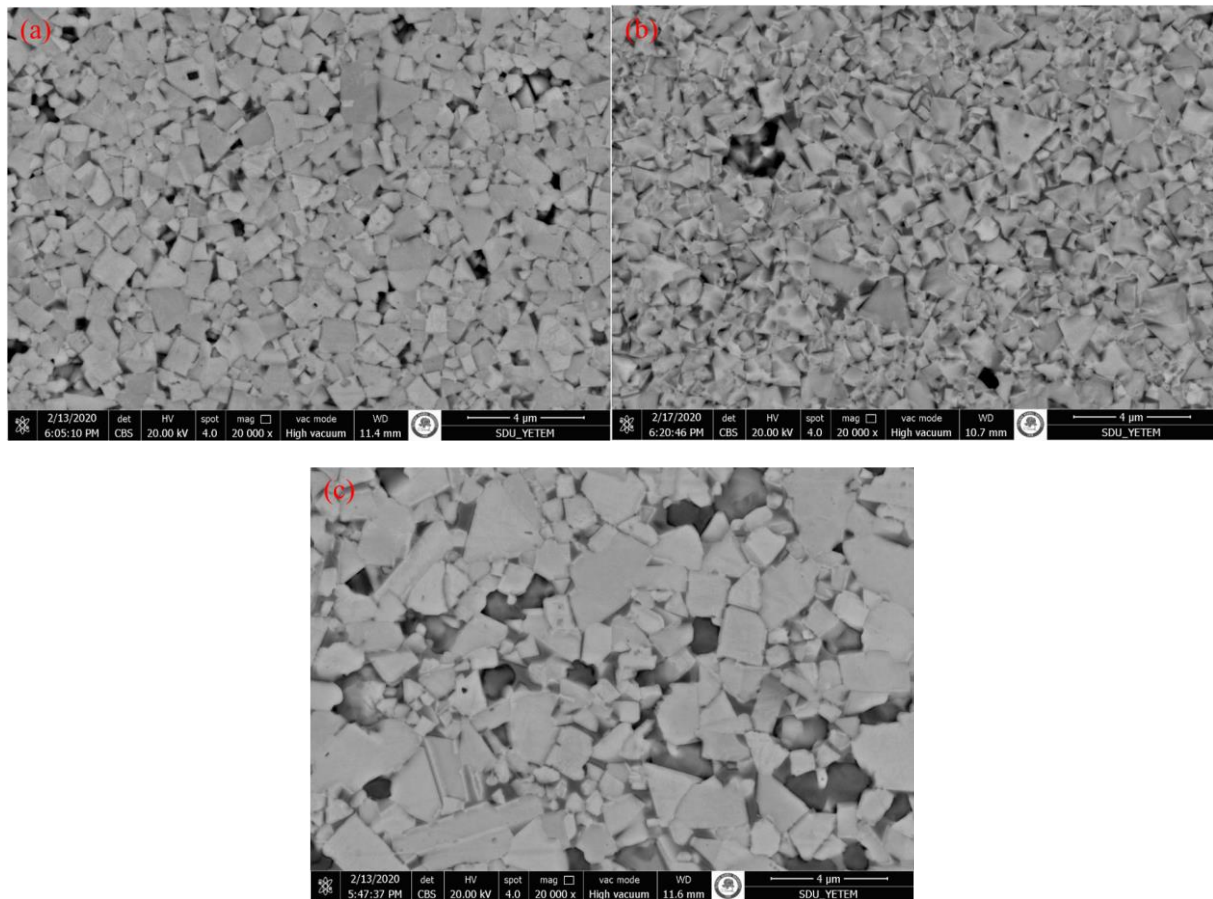


Figure 1. Cutting inserts microstructures: (a) Uncoated, (b) AlTiN coated, and (c) TiCN-Al₂O₃

In sintered cemented carbides, the α -phase (WC) can be found as prismatic grains while the β -phase (cobalt binder) can be found as white veins in the microstructure. Moreover, A sub-stoichiometric carbide phase called η -phase (Co₃W₃C (M6C) and (Co₆W₆C (M12C)) can form in the microstructure. This phase tends to decrease the toughness of cemented carbides, especially if it precipitates as large dendrites [26]. As can be seen in Fig.1, the α phase (WC) is mostly in the form of gray and prismatic grains and the η -phase is in the form of dark gray flecks [9]. According to the microstructure images, the Wc grains of the cutting tools are different from each other. Especially, it is seen that the grain size is smaller in the single-layer (AlTiN) coated insert compared to the uncoated and two-layer (TiCN-Al₂O₃) coated cutting tools. The hardness or toughness of a cutting tool is characterized by WC grain size and Co content. These properties can be changed depending on the material and type of application [26]. Therefore, the WC grain size is different. It is also seen that the multiple complex carbides dimensions are larger in the microstructure of the two-layer (TiCN-Al₂O₃) coated cutting insert.

Table 1. Cutting parameters and levels

Symbol	Cutting Parameters	Level		
		I	II	III
Ct	Cutting tool	Uncoated	AlTiN	TiCN-Al ₂ O ₃
Vc	Cutting speed (m/min)	40	60	80
f	Feed rate (mm/rev)	0.08	0.12	0.16
a	Depth of cut (mm)	0.6		

2.2 Experimental measurement system and procedures

The three force components -the main cutting force (Fc), the feed force (Ff), and the radial force (Fr) that appeared in the turning machining of the test materials were measured with a KISTLER 9257B type piezoelectric dynamometer. In the analysis of cutting forces, the main cutting force (Fc) values, which are of primary importance in terms of energy consumption in machining operations, are primarily considered. The schematic view of the experimental setup is given in Figure 2.

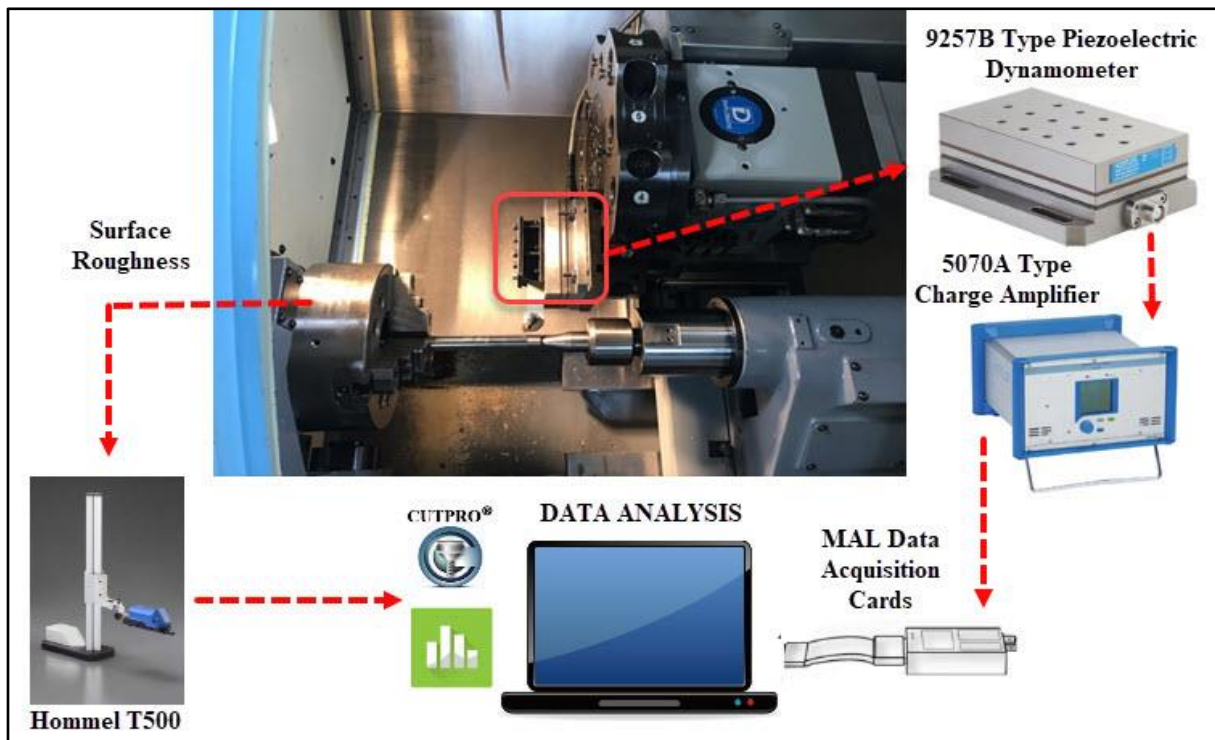


Figure 2. Experimental setup

After each turning experiment, workpiece surface roughness was measured with the HOMMEL Tester T 500 device. By axially rotating the workpiece, three different measurements were taken on three machined surfaces at each 120° . The average surface roughness (R_a) values were calculated with the arithmetic averages of the obtained values. On the other hand, the formation of flank wear (V_b) was measured using a Insize toolmaker's ISM-PM200SA digital microscope (having resolution:1600x1200 and magnification up to 200x)

Uniform flank wear value has been chosen as 0.3 mm accordingly to the ISO-3685 standards [27]. A new insert has been used for each turning experiment. The trial test has been made until the flank wear (V_b) of 0.3 mm and then, a comparison of tool life was made considering the longest cutting time. In addition, the worn inserts were analyzed using Quanta FEG 250 Scanning Electron Microscopy (SEM). The mathematical model used in power consumption calculations is shown in Eq. (1). The power consumption was determined according to the main cutting forces measured in experiments performed under all cutting conditions using this equation.

$$P = F_c \times V_c / 60 \quad (1)$$

3. Optimization Process

The different optimization methods are used in the manufacturing industry to minimize product costs and improve the production process. The Taguchi method, which is an optimization method, is widely used in engineering analysis. This method significantly reduces the number of tests using orthogonal arrays. Moreover, it minimizes the effects of uncontrollable factors that are not considered in traditional experimental design [22]. The test results are converted to Signal-to-Noise (S/N) ratio in this method. The term signal (S) refers to the desired values from the system, and the term noise (N) refers to the factors that are not considered in the experimental design but affect the test results [9]. The goal of this study is to minimize output parameters (F_c , R_a , V_b , and P_c). Therefore, the equation corresponding to the lower-the-better approach in Eq. (2) was used to calculate the S/N ratios.

$$n = \frac{S}{N} = -10 \log \left(\frac{1}{n} \sum_{i=1}^n y_i^2 \right) \quad (2)$$

The most suitable orthogonal array L27 (3^3) has been used in the preparation of the experimental design to determine the ideal process factors. Cutting tools (uncoated, PVD-AlTiN, PVD-TiCN- Al_2O_3), cutting speed (V_c), and feed rate (f) have been selected as machining factors.

Furthermore, variance analysis has been applied to analyze the impacts of processing factors, while regression analysis was used to express the relationship between output and input parameters numerically. Finally, the accuracy of the optimization process was tested at the optimum and random processing levels.

4. Results and Discussion

4.1 Cutting Force

The influences of the used cutting tool coatings on F_c were investigated. Figure 3 shows the variation of the measured F_c values when machining Invar 36 alloy with different (uncoated, AlTiN and TiCN-Al₂O₃) coated cutting tools. At all cutting conditions, the single layer (AlTiN) coated inserts show better F_c upto average 15% than uncoated inserts. Furthermore, two-layer (TiCN-Al₂O₃) coated inserts are better than AlTiN coated inserts and uncoated inserts as 9% and 20%, respectively. The lowest F_c has been measured as 180N in two-layer (TiCN-Al₂O₃) coated inserts irrespective of cutting speed. At the same cutting conditions (80 m/min and 0.08 mm/rev), F_c was measured at 260 and 285 N for AlTiN coated inserts and uncoated inserts, respectively. Thakur et al. were associated this situation with the thermal conductivity of the cutting tools [28]. The two-layer (TiCN-Al₂O₃) coated inserts have a better ability to dissipate heat to the environment, resulting in superior performance. Moreover, two-layer (TiCN-Al₂O₃) coated inserts made high-speed machining possible, reducing cutting force. As can be deduced from Figure 3 (c), in the experiments with these cutting tools, it is an indication of this situation that the cutting force values decrease significantly with the increase in cutting speed. For example, in experiments performed at cutting speeds of 40, 60, and 80 m/min, F_c was measured at 280, 265, and 180 N, respectively. On the other hand, SEM pictures are further proof of the better strength of this cutting tool. SEM pictures in Fig. 4 show the worn inserts at the end of machining Invar 36 alloy with three different cutting inserts at a feed rate of 0.16 mm/rev, a cutting speed of 80 m/min, and a depth of cut of 0.6 mm. F_c values decreased by approximately 35.74%. On the other hand, SEM pictures are further proof of the better strength of this cutting tool. The SEM images of the inserts in Fig. 4 reveal dominant wear mode of the uncoated and coated cutting inserts was found to be Vb and built-up-edge (BUE). there is also a negligible edge chipping. Particularly, abrasive marks and the size of

BUE in the uncoated insert is higher than those of the single-layer (AlTiN) and two-layer (TiCN-Al₂O₃) coated inserts.

It can be deduced from these images that the abrasive wear mechanism is effective on uncoated cutting tools while adhesion (BUE) is effective on coated cutting tools. Abrasive wear and BUE formation in cemented carbide cutting tools in machining of superalloys were also reported by other researchers [29, 30].

4.2 Surface Roughness

Surface roughness is a crucial factor for defining the surface quality of workpieces in manufacturing processes. The surface condition affects various tribological properties such as friction, heat conduction, coating, oil retention, fatigue strength, corrosion resistance, which cause wear of a product under operating conditions [31]. Therefore, it is all-important to determine the ideal levels of parameters, such as V_c , f , a_p , and tool geometry, which directly affect the R_a to get the desired surface quality of a part during machining. the R_a values for various cutting tool coatings are seen Fig. 5. The R_a values ranged from 0.85 to 2.38 μm . It is showed that the surface roughness in tests performed using a two-layer (TiCN-Al₂O₃) coated insert is remarkably lower than the uncoated and the single-layer (AlTiN) coated inserts. As can be seen from Fig. 4, this situation could be associated with the lower wear occurring in the two-layer (TiCN-Al₂O₃) coated insert according to uncoated and the single-layer (AlTiN) coated inserts. The wear mechanisms in the cutting tool affect the surface roughness was also reported by other researchers [24, 32, 33]. For instance, in a study on the turning of AISI D2 steel with PVD and CVD coated inserts, it was reported that lower flank wear in the PVD coated insert positively affects the surface quality [34].

Moreover, when Figure 5 is examined, generally, surface roughness values are high at low cutting speeds. The R_a values slightly decreased with the increase in V_c . However, it is seen that the R_a values are more affected by the f than the V_c . When the R_a values measured in the experiments performed with uncoated inserts at 40 m/min cutting speed, 0.6 mm depth of cut, and three feed rates are compared, the R_a values increased approximately by 15% and 20%, respectively, in 0.12 mm/rev and 0.16 mm/rev compared to 0.08 mm/rev. A similar increasing trend has indicated in other cutting tools.

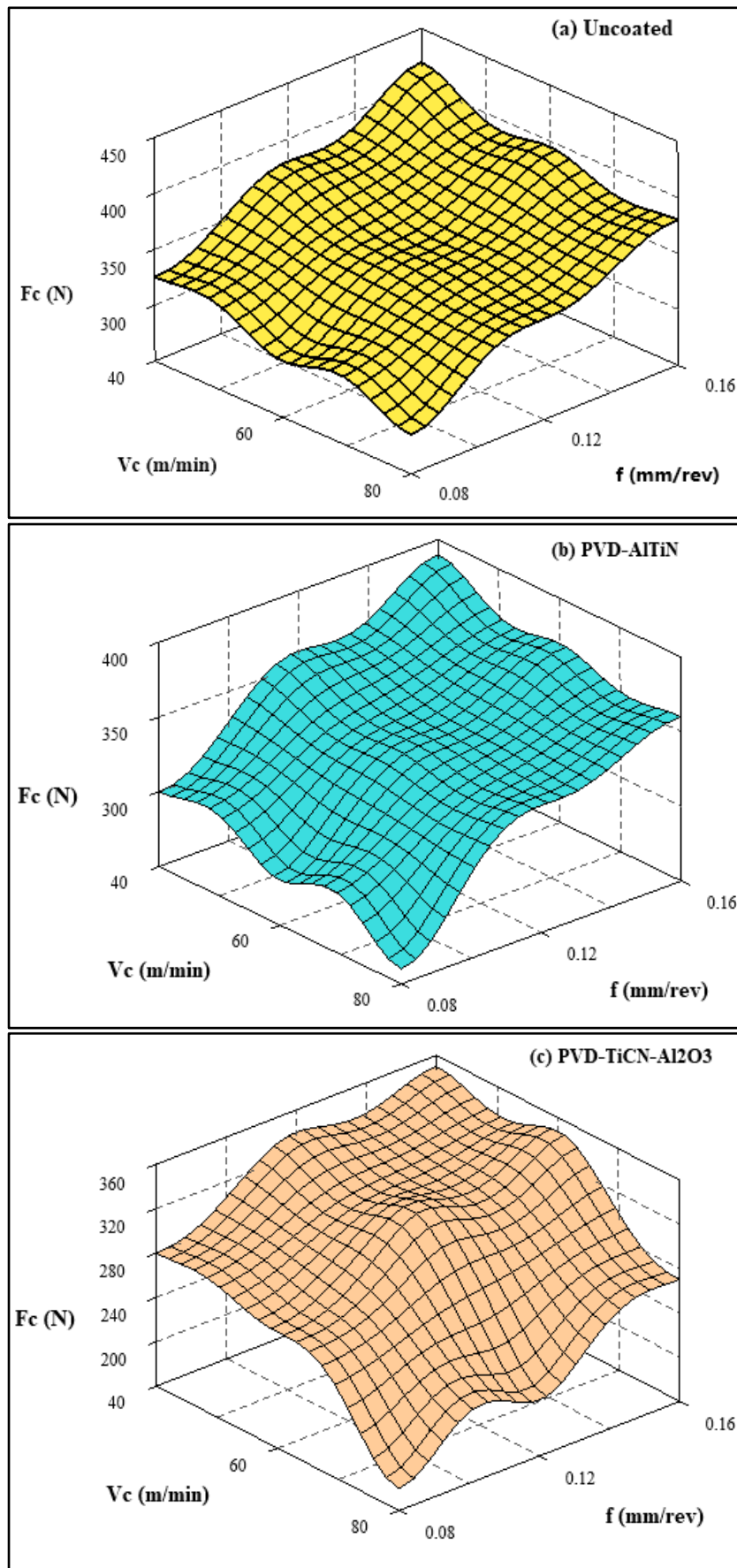


Figure 3. Cutting force variations based on cutting parameters

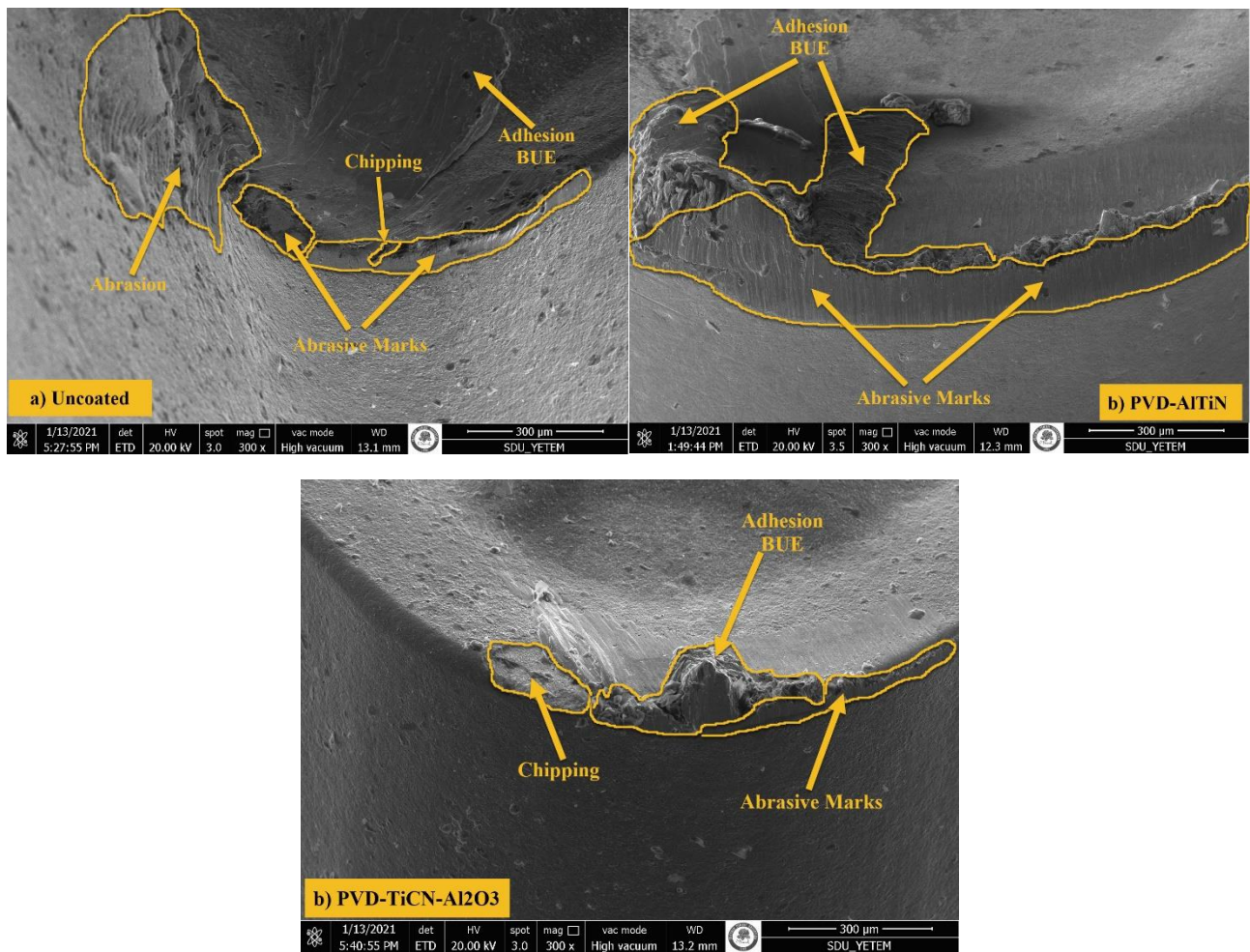


Figure 4. SEM images of worn cutting inserts at the end of Invar 36 cutting

However, with a two-layer ($\text{TiCN-Al}_2\text{O}_3$) coated insert, this increase is less than the uncoated and the single-layer (AlTiN) coated inserts. The best surface roughness values were achieved in the experiments performed with two-layer ($\text{TiCN-Al}_2\text{O}_3$) coated insert.

4.3 Tool Wear

The wear mechanisms in the cutting tools have been examined to define the influence of the coating type on the cutting performance, and as a result, flank wear was found as the dominant wear type. Thus, the flank wear formation in cutting tools was analyzed. Figure 6 shows the variation of the flank wear measured in the cutting tools as a result of the experiments carried out at a constant feed rate of 0.08 mm/rev and cutting speeds of 40 m/min, 60 m/min, and 80 m/min. The evolution of V_b was defined by cutting time. As can be seen from Fig. 6, the flank wear increases as the cutting speed increases, which the cutting tool reaches the wear limit (0.3 mm) earlier. This situation could be associated with the tool wear being significantly accelerated due to the formation of high cutting temperatures with an increase in V_c , and therefore the

tool life is shortened. The low thermal conductivity of the Invar 36 alloy can also effectively accelerate tool wear at high cutting speeds, so the cutting tool is subject to high heat transfer from the cutting zone and may prematurely lose cutting life due to rapid wear.

Considering the effect of the cutting tool coating according to Figure 6, it is seen that the wear process of the tool accelerates with the increase in V_c in all tools, but this wear time is slightly longer in coated tools compared to the uncoated tool. To elaborate, the two-layer ($\text{TiCN-Al}_2\text{O}_3$) coated insert enhanced tool life about 30% and 60% compared to the single-layer (AlTiN) coated and uncoated inserts in the machining of Invar 36, respectively.

4.4 Power Consumption

Figure 7 shows the P_c values for various cutting tool coatings in the turning of Invar 36 alloy. As can be seen from Fig. 7, the f and V_c increment have an increasing effect on P_c .

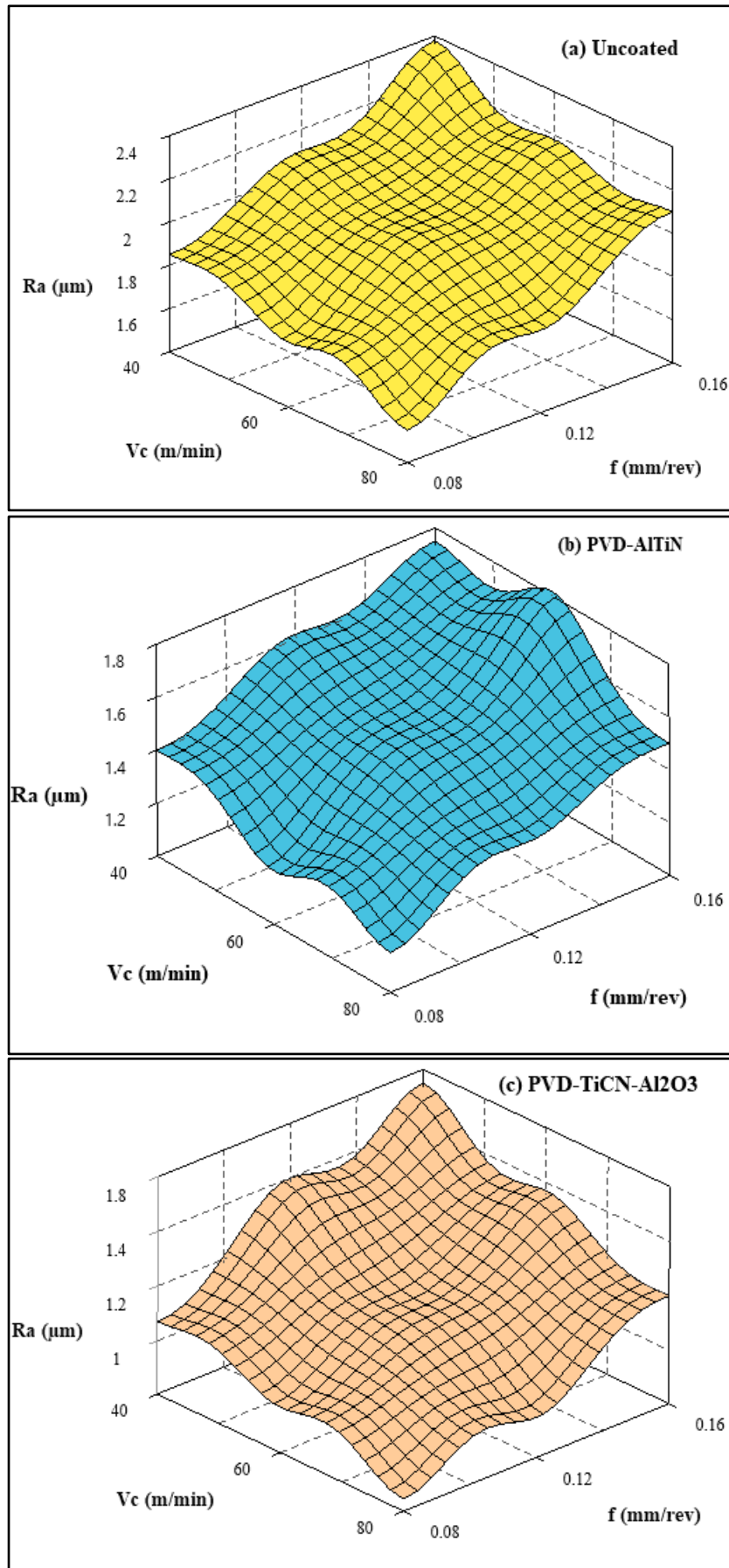


Figure 5. Surface roughness variations based on cutting parameters.

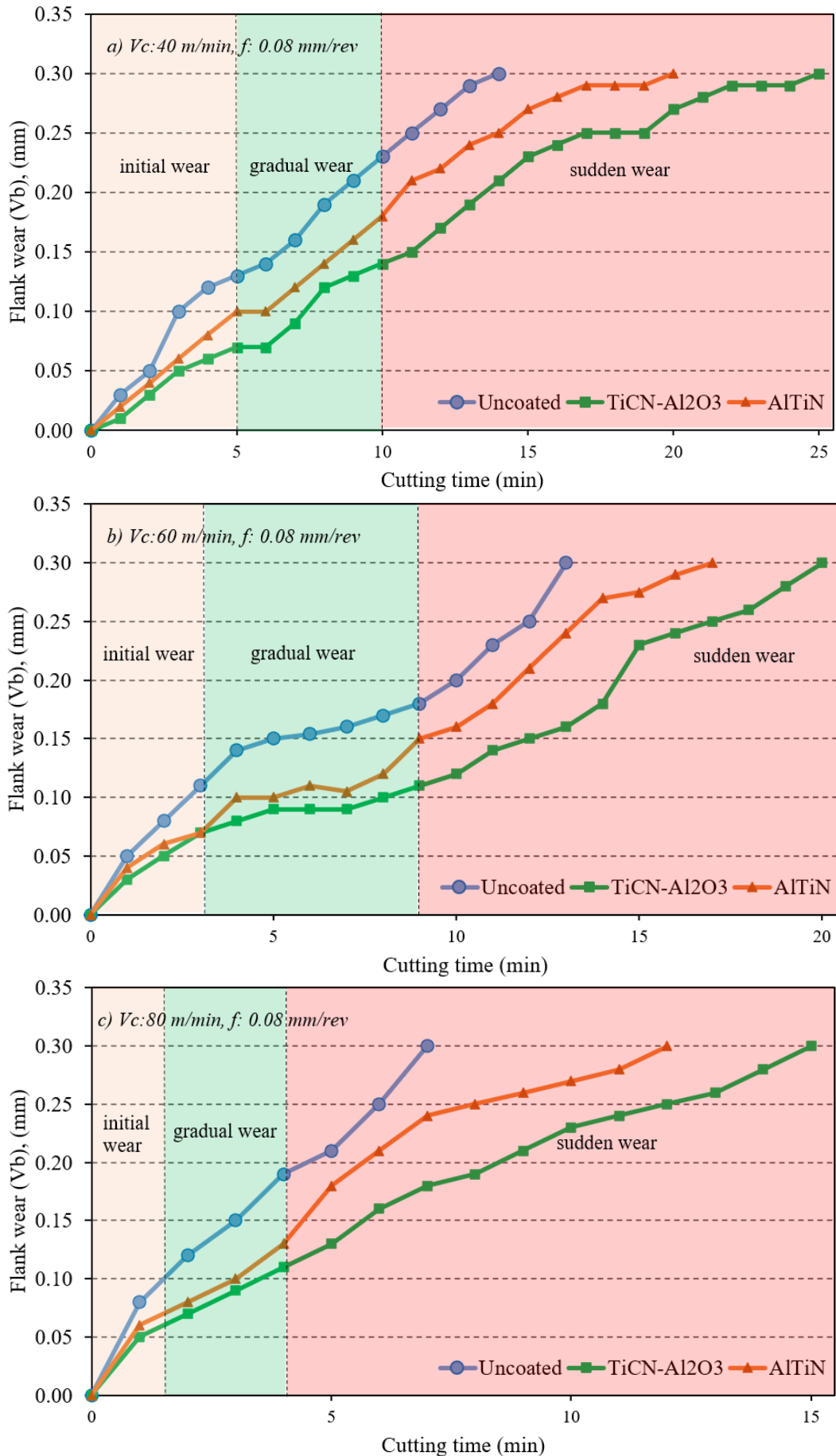


Figure 6. Evolution of tool wear based on cutting parameters

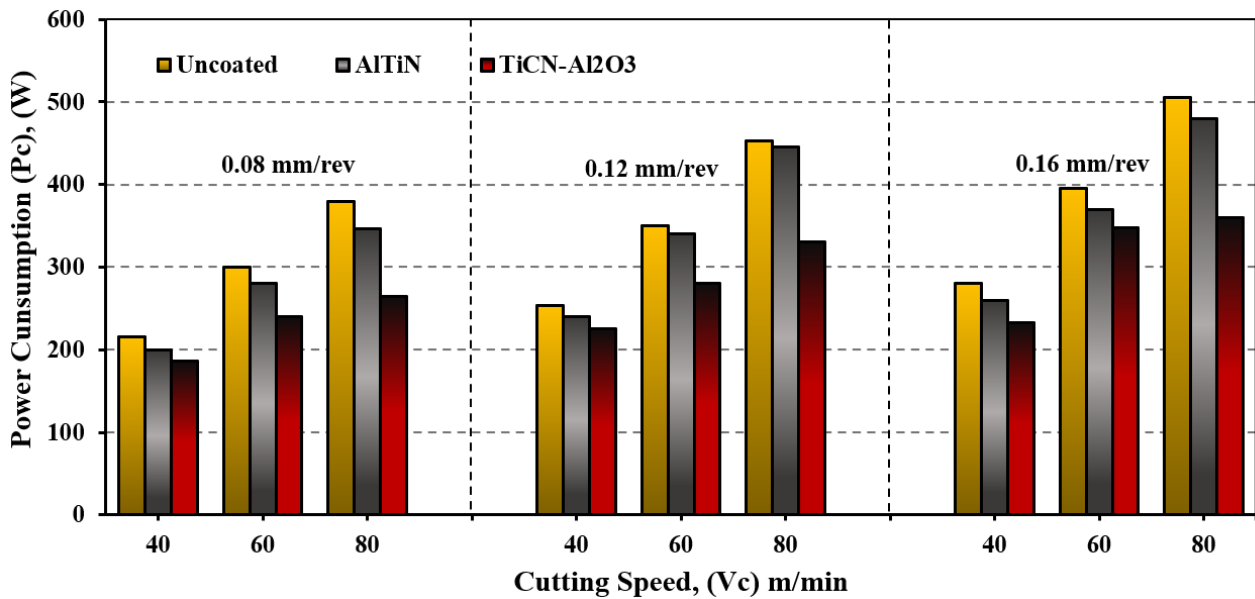


Figure 7. Power consumption variations based on cutting parameters

When Figure 7 is examined, it shows that P_c increased about 50 and 40% with increasing V_c from 40 to 60 m/min and 60 to 80 m/min, respectively, under all cutting conditions. As can be derived from Eq. 1, it is expected that the P_c will increase with the increase in V_c . Considering the effect of the feed rate, the P_c also increased owing to the increase in F_c as the chip cross-section increased due to the rise in the f . On the other hand, as can be deduced Fig. 7, the P_c in the machining of Invar 36 using two-layer (TiCN-Al₂O₃) coated insert is lower in comparison with uncoated and the single-layer (AlTiN) coated inserts. The notable reason for improvements under a two-layer (TiCN-Al₂O₃) coated insert could be the decrease in V_b and F_c due to the increase in the thermal resistance of the cutting tool. The lowest P_c was acquired with a two-layer (TiCN-Al₂O₃) coated insert at the feed rate of 0.08 mm/rev, the depth of cut of 0.6 mm, and the cutting speed of 40 m/min.

4.5 Optimization of Output Parameters

The output parameters represented by the cutting force (F_c), the surface roughness (R_a), the tool wear (V_b), and the power consumption (P_c) obtained at the machining of Invar 36 are given in Table 2. Taguchi S/N response table was used to determine the optimal levels of cutting parameters on the output parameters (F_c , R_a , V_b , and P_c). The S/N response for the output parameters are seen in Table 3. In the table, the level with the highest S/N value is considered determining the optimum cutting parameter, and the data shown in bold in the table highlight significant levels of cutting parameters. As can be deduced in Tables 2 and 3, the

ideal input parameters levels for the F_c and R_a were found to be a two-layer (TiCN-Al₂O₃) coated insert, a cutting speed of 80 m/min, and the feed rate of 0.08 mm/rev. Similarly, the ideal input parameters for the V_b and P_c were specified as a two-layer (TiCN-Al₂O₃) coated insert, the cutting speed of 40 m/min, and the feed rate of 0.08 mm/rev.

4.6 Variance Analysis of Output Parameters

Analysis of variance has been applied to determine the effects of cutting parameters on the output parameters. Analysis results are given in Table 4. In the table, the significance level (P) and contribution ratio (F) values were considered. The P -value must be less than 0.05 for the cutting parameters to be significant for the outputs. The factor with the highest F value is also accepted as the most efficient factor. The best influential factors on F_c and R_a are the f with 44.59% additive rate and the cutting tool coating with 67.14% additive rate, respectively, as can be seen in Table 4. Similarly, the most influential parameters on V_b and P_c are the cutting speed with 44.59% and 67.14% additive rate, respectively.

4.7 Regression Analysis of Output Parameters

The linear and second-degree regression model is developed to predict the output parameters (F_c , R_a , V_b , and P_c) without needs for the experiments. The mathematical models are the linear-degree regression models for the output parameters (F_c , R_a , V_b , and P_c) shown in Eqn. 3-6, respectively.

$$F_{cT} = 343.5 - 33.44Ct - 1.458Vc + 1122f \quad (3)$$

Table 2. Experiment results

Test Id	Parameters										
	A (Ct)	B (Vc)	C (f)	Fc (N)	Fc-S/N (dB)	Ra (µm)	Ra-S/N (dB)	Vb (mm)	Vb-S/N (dB)	Pc (W)	Ra-S/N (dB)
1	1	40	0.08	325	-50.237	1.85	-5.3434	0.22	13.1515	216	-46.6891
2	1	40	0.12	380	-51.595	2.10	-6.4443	0.24	12.3957	253	-48.0624
3	1	40	0.16	420	-52.465	2.38	-7.5315	0.26	11.7005	280	-48.9432
4	1	60	0.08	300	-49.542	1.70	-4.6089	0.23	12.7654	300	-49.5424
5	1	60	0.12	350	-50.881	2.00	-6.0206	0.25	12.0412	350	-50.8814
6	1	60	0.16	395	-51.931	2.18	-6.7691	0.26	11.7005	395	-51.9319
7	1	80	0.08	285	-49.096	1.55	-3.8066	0.26	11.7005	380	-51.5957
8	1	80	0.12	340	-50.629	1.78	-5.0084	0.28	11.0568	453	-53.1220
9	1	80	0.16	380	-51.595	2.10	-6.4443	0.30	10.4575	506	-54.0830
10	2	40	0.08	300	-49.542	1.40	-2.9225	0.17	15.3910	200	-46.0206
11	2	40	0.12	360	-51.126	1.62	-4.1903	0.18	14.8945	240	-47.6042
12	2	40	0.16	390	-51.821	1.75	-4.8607	0.20	13.9794	260	-48.2995
13	2	60	0.08	280	-48.943	1.20	-1.5836	0.20	13.9794	280	-48.9432
14	2	60	0.12	340	-50.629	1.50	-3.5218	0.23	12.7654	340	-50.6296
15	2	60	0.16	370	-51.364	1.82	-5.2014	0.24	12.3957	370	-51.3640
16	2	80	0.08	260	-48.299	1.15	-1.2139	0.24	12.3957	346	-50.7815
17	2	80	0.12	335	-50.500	1.35	-2.6066	0.26	11.7005	446	-52.9867
18	2	80	0.16	360	-51.126	1.50	-3.5218	0.30	10.4575	480	-53.6248
19	3	40	0.08	280	-48.943	1.07	-0.5876	0.12	18.4163	186	-45.3903
20	3	40	0.12	340	-50.629	1.40	-2.9225	0.13	17.7211	226	-47.0822
21	3	40	0.16	350	-50.881	1.55	-3.8066	0.16	15.9176	233	-47.3471
22	3	60	0.08	265	-48.464	0.97	0.2645	0.15	16.4781	240	-47.6042
23	3	60	0.12	330	-50.370	1.15	-1.2139	0.19	14.4249	280	-48.9432
24	3	60	0.16	348	-50.831	1.37	-2.7344	0.20	13.9794	348	-50.8316
25	3	80	0.08	180	-45.105	0.85	1.4116	0.20	13.9794	265	-48.4649
26	3	80	0.12	210	-46.444	0.95	0.4455	0.25	12.0412	330	-50.3703
27	3	80	0.16	270	-48.627	1.20	-1.5836	0.30	10.4575	360	-51.1261

Table 3. S/N response of experiment results

	Cutting factors					
	A (Ct)	B (Vc)	C (f)	A (Ct)	B (Vc)	C (f)
<i>Fc</i>						
1	-50.89	-50.80	-48.69	-5.775	-4.290	-2.043
2	-50.37	-50.33	-50.31	-3.291	-3.488	-3.498
3	-48.92	-49.05	-51.18	-1.192	-2.481	-4.717
Delta	1.96	1.76	2.50	4.583	1.809	2.674
<i>Vb</i>						
1	11.89	14.84	14.25	-50.54	-47.27	-48.34
2	13.11	13.39	13.23	-50.03	-50.07	-49.96
3	14.82	11.58	12.34	-48.57	-51.79	-50.86
Delta	2.94	3.26	1.91	1.97	4.52	2.50
<i>Pc</i>						

Table 4. Result of variance for the output parameters

Factors	Degree of freedom (DoF)	Sum of squares (SS)	Mean square (MS)	F ratio	P ratio	Contribution rate (%)
<i>Fc</i>						
Ct	2	21218	10609	23.82	0.000	25.50
Vc (m/min)	2	15988	7994	17.95	0.000	19.21
f (mm/rev)	2	37103	18551.3	41.65	0.000	44.59
Error	20	8907	445.4			10.70
Total	26	83216				100
<i>Ra</i>						
Ct	2	2.86992	1.43496	456.29	0.000	67.14
Vc (m/min)	2	0.40299	0.20149	64.07	0.000	9.43
f (mm/rev)	2	0.93867	0.46934	149.24	0.000	21.96
Error	20	0.06290	0.00314			1.47
Total	26	4.27447				100
<i>Vb</i>						
Ct	2	0.020030	0.010015	30.73	0.000	30.64
Vc (m/min)	2	0.028541	0.014270	43.78	0.000	43.67
f (mm/rev)	2	0.010274	0.005137	15.76	0.000	15.72
Error	20	0.006519	0.000326			9.97
Total	26	0.065363				100
<i>Pc</i>						
Ct	2	26500	13250	20.07	0.000	13.36
Vc (m/min)	2	120722	60385.8	91.45	0.000	60.87
f (mm/rev)	2	37940	18970	28.73	0.000	19.12
Error	20	13206	660.3			6.66
Total	26	198417				100

$$Ra_l = 2.0904 - 0.3961Ct - 0.007472Vc + 5.708f \quad (4)$$

$$Vb_l = 0.0996 - 0.0333Ct + 0.001972Vc + 0.597f \quad (5)$$

$$Pc_l = 9.2 - 36.94Ct + 4.089Vc + 1137f \quad (6)$$

In the regression analysis, the coefficients of determination (R^2), which is a statistical measure of how close the data are to the appropriate regression line, was taken into account [35]. The R^2 value is always between 0 and 100%, and the higher the (R^2) value, the better the model usually complies with the data. The R^2 are found as 86.18%, 97.43%, 89.16%, and 91.83% for the F_c , R_a , V_b , and P_c , respectively. On the other hand, the mathematical models are the second-degree regression models for the output parameters (F_c , R_a , V_b , and P_c) shown in Eqn. 7-10, respectively. Moreover, the R^2 are found as 93.18%, 98.79%, 98.05%, and 98.11% for the F_c , R_a , V_b , and P_c , respectively. the high (R^2) values of second-degree models compared to linear models indicate that it largely explains the variability of the response data

around the mean. The deviation between the experimental and predicted values for the output parameters is seen in Figure 8. As can be deduced Fig. 8, the experimental and predicted values are very close to each other.

$$F_{c_q} = 19 + 78.3Ct + 2.93Vc + 2876f - 13.44Ct^2 - 0.0265Vc^2 - 7361f^2 - 0.792Ct * Vc - 88Ct * f + 3.12Vc * f \quad (7)$$

$$R_{a_q} = 1.916 - 0.633Ct - 0.00126Vc + 8.69f + 0.0872Ct^2 - 0.000032Vc^2 - 3.8f^2 - 0.0005Ct * Vc - 0.688Ct * f - 0.0115Vc * f \quad (8)$$

$$V_{b_q} = 0.3838 - 0.0994Ct - 0.00382Vc - 0.215f - 0.00222Ct^2 + 0.000024Vc^2 - 0.35f^2 + 0.000917Ct * Vc + 0.1667Ct * f + 0.00938Vc * f$$

$$P_{c_q} = -226.1 + 113.6Ct + 6.56Vc + 1725f - 17.94Ct^2 - 0.0203Vc^2 - 6632f^2 - 1.167Ct * Vc - 73Ct * f + 19.17Vc * f \quad (10)$$

4.8 Confirmation Experiments

The final stage of the optimization process is to perform validation experiments at optimal and random levels to check the accuracy of the optimization. To see the success of the optimization, the confidence intervals (CI) have been calculated for the output parameters (Fc, Ra, Vb, and Pc) according to Eqn. (11, 12). The explanations of the symbols in Eqn. (11, 12) are given in the Abbreviations section. $F_{0.05,1,20} = 4.3512$ (From F test table), $Ve_{Fc} = 445.4$, $Ve_{Ra} = 0.00314$, $Ve_{Pc} = 660.3$ and $Ve_{Vb} = 0.000326$ (Table 4), $R = 1$ $N = 27$ $T_{dof} = 6$ and $n_{eff} = 3.857$ (Eq. (11)). CI_{Fc} , CI_{Ra} , CI_{Vb} , and CI_{Pc} were calculated as 49.401, 0.131, 0.042 and 60.148 by using Eq. (12), respectively.

$$n_{eff} = \frac{N}{1+T_{dof}} \tag{11}$$

$$CI_{Ra\ Fc\ P} = \sqrt{F_{a,1,fe} V_e \left[\frac{1}{n_{eff}} + \frac{1}{R} \right]} \tag{12}$$

As can be deduced in Table 3, the ideal level groups for the lowest Fc, Ra, Vb, and Pc are A3B3C1, A3B3C1, A3B1C1, and A3B1C1, respectively. The estimated optimum values were calculated using the models shown in Eqn. 13-16, respectively.

$$Fc_{opt} = (A_3 - T_{Fc}) + (B_3 - T_{Fc}) + (C_1 - T_{Fc}) + T_{Fc}$$

$$Ra_{opt} = (A_3 - T_{Ra}) + (B_3 - T_{Ra}) + (C_1 - T_{Ra}) + T_{Ra}$$

$$Vb_{opt} = (A_3 - T_{Vb}) + (B_1 - T_{Vb}) + (C_1 - T_{Vb}) + T_{Vb}$$

$$Pc_{opt} = (A_3 - T_{Pc}) + (B_1 - T_{Pc}) + (C_1 - T_{Pc}) + T_{Pc}$$

T_{Fc} , T_{Ra} , T_{Vb} , and T_{Pc} are the average of the values obtained in the experiments for each output parameter. T_{Fc} , T_{Ra} , T_{Vb} , and T_{Pc} are calculated to be 323.81 N, 1.534 μm , 0.222 mm, and 317.148 W, respectively. As a result of the calculations, Fc_{opt} , Ra_{opt} , Vb_{opt} , and Pc_{opt} are found to be 302 N, 0.785 μm , 0.1305 mm, and 140.704 W, respectively.

$$[Fc_{opt} - CI_{Fc}] < Fc_{exp} < [Fc_{opt} + CI_{Fc}] = [302 - 49.401] < 180 < [302 + 49.4] = 252.599 < 180 < 351.4$$

$$[Ra_{opt} - CI_{Ra}] < Ra_{exp} < [Ra_{opt} + CI_{Ra}] = [0.785 - 0.131] < 0.85 < [0.785 + 0.131] = 0.654 < 0.85 < 0.916$$

$$[Vb_{opt} - CI_{Vb}] < Vb_{exp} < [Vb_{opt} + CI_{Vb}] = [0.1305 - 0.042] < 0.12 < [0.1305 + 0.042] = 0.088 < 0.12 < 0.1725$$

Table 5. The verification test results

Level	Taguchi method			Linear regression equations			Quadratic regression equations		
	Exp.	Pred.	Error (%)	Exp.	Pred.	Error (%)	Exp.	Pred.	Error (%)
Fc (N)									
A ₃ B ₃ C ₁	180	175.14	2.70	180	206.3	14.61	180	189.47	5.26
A ₁ B ₂ C ₃	395	393.03	0.50	395	402	1.77	395	404.33	2.36
Ra (μm)									
A ₃ B ₃ C ₁	0.85	0.828	2.58	0.85	0.76	10.58	0.85	0.808	4.94
A ₁ B ₂ C ₃	2.18	2.24	2.75	2.18	2.15	1.37	2.18	2.22	1.83
Vb (mm)									
A ₃ B ₁ C ₁	0.12	0.11	8.33	0.12	0.126	5.00	0.12	0.111	7.50
A ₂ B ₂ C ₁	0.20	0.202	1.00	0.20	0.199	0.50	0.20	0.195	2.19
Pc (W)									
A ₃ B ₁ C ₁	186	188.14	1.15	186	152.9	17.79	186	182.49	1.88
A ₂ B ₂ C ₁	280	276.03	1.41	280	271.6	2.99	280	285.71	2.03

$$[P_{c_{opt}} - CI_{Pc}] < P_{c_{exp}} < [P_{c_{opt}} + CI_{Pc}] = [140.704 - 60.148] < 186 < [140.704 + 60.148] = 80.556 < 186 < 200.852$$

The values obtained at the optimum process parameters for all output are within the confidence interval limits. This is an indication of the correctness of the optimization process. Moreover, the accuracy of the optimization process was tested at the optimum and random levels of the input factors and the results are given in Table 5. The requirement for error values to be less than 20% for reliable statistical analysis was reported by other researchers [22, 36, 37]. As summarized in Table 5, the deviation values are within acceptable limits, which proves that the optimization process has been carried out successfully

4. Conclusion

This paper has presented a comparison of the performance of uncoated, the single-layer (AlTiN), and a two-layer (TiCN-Al₂O₃) coated inserts in machining of Invar 36 alloy in different cutting conditions. The cutting performance of these tools has been compared regarding Fc, Ra, Vb, and Pc. Moreover, these output parameters have been modeled by determining the optimum cutting conditions by applying Taguchi method, Anova analysis, and regression analysis. Based on the experimental and statistical results obtained, the following conclusions can be drawn:

- The two-layer (TiCN-Al₂O₃) coated insert was increased tool life up to about 30% and 60% compared to the single-layer (AlTiN) coated and uncoated inserts, respectively.
- The flank wear and built-up-edge (BUE) were observed as the dominant wear modes for all the cutting tools.
- The cutting time decreased significantly with the increasing cutting speed in all tools in the machining of Invar 36 alloy.
- Cutting force and surface roughness values decrease in experiments with two-layer (TiCN-Al₂O₃) coated inserts compared to single-layer (AlTiN) coated and uncoated inserts.
- Two-layer (TiCN-Al₂O₃) and single-layer (AlTiN) coated inserts according to uncoated insert provided 10.22% and 3.77% reduction in power consumption, respectively.

- The output parameters (Fc, Ra, Vb, and Pc) increased depending on the increasing feed rate.
- The Taguchi analysis showed that the ideal level groups for the lowest Fc, Ra, Vb, and Pc were A3B3C1, A3B3C1, A3B1C1, and A3B1C1, respectively.
- Statistical analysis results showed that the most influential parameters on Fc and Ra were the feed rate with 44.59% additive rate and the cutting tool coating with 67.14% additive rate, respectively. Similarly, the most influential parameters on Vb and Pc were the cutting speed with 44.59% and 67.14% additive rate, respectively.
- First and second-order models developed to estimate the output parameters (Fc, Ra, Vb, and Pc) give successful results with high coefficients of determination (R²).

According to all of these results above, in the machining of materials such as Invar 36 alloy, which has a low thermal conductivity coefficient, it is recommended to select the cutting parameters at medium levels and use multi-layer cutting tools in order not to lose the cutting tool performance prematurely.

Abbreviations

Fc	Cutting force
Ra	Surface roughness
Vb	Tool wear
Pc	Power consumption
F_{α,1,fe}	The F ratio at a 95% confidence
α	The significance level
fe	The degrees-of-freedom of error
Ve	Error variance
R	The number of replications for confirmation experiments
N	The total number of experiments
n_{eff}	The effective number of replications

References

- [1] Midilli, A.; Dincer, I.; Key strategies of hydrogen energy systems for sustainability. *Int J Hydrogen Energy.*, 2007, 32, 511–524. <https://doi.org/10.1016/J.IJHYDENE.2006.06.050>
- [2] Salem, A.; Hegab, H.; Kishawy, H. A.; An integrated approach for sustainable machining processes: Assessment, performance analysis, and optimization. *Sustain Prod Consum.*, 2021, 25, 450–470. <https://doi.org/10.1016/J.SPC.2020.11.021>
- [3] Jayal, A. D.; Badurdeen, F.; Dillon, O. W.; Jawahir, I. S.; Sustainable manufacturing: Modeling and optimization challenges at the product, process and system levels. *CIRP J Manuf Sci Technol.*, 2010, 2, 144–152. <https://doi.org/10.1016/J.CIRPJ.2010.03.006>
- [4] López De Lacalle, L. N.; Angulo, C.; Lamikiz, A.; Sánchez, J. A.; Experimental and numerical investigation of the effect of spray cutting fluids in high speed milling. *J Mater Process Technol.*, 2006, 172, 11–15. <https://doi.org/10.1016/J.JMATPROTEC.2005.08.014>
- [5] Aslan, D.; Budak, E.; Semi-analytical Force Model for Grinding Operations. *Procedia CIRP*, 2014, 14, 7–12. <https://doi.org/10.1016/J.PROCIR.2014.03.07372>.
- [6] Akgün, M.; Demir, H.; Estimation of surface roughness and flank wear in milling of Inconel 625 superalloy. *Surf Rev Lett* 2021, 28, 2150011. <https://doi.org/10.1142/S0218625X21500116>
- [7] Korkmaz, M. E.; Gupta, M. K.; Boy, M.; et al.; Influence of duplex jets MQL and nano-MQL cooling system on machining performance of Nimonic 80A. *J Manuf Process.*, 2021, 69, 112–124. <https://doi.org/10.1016/J.JMAPRO.2021.07.039>
- [8] Şirin, Ş.; Yıldırım, Ç. V.; Kıvak, T.; Sarıkaya, M.; Performance of cryogenically treated carbide inserts under sustainable cryo-lubrication assisted milling of Inconel X750 alloy. *Sustain Mater Technol.*, 2021, 29, e00314. <https://doi.org/10.1016/J.SUSMAT.2021.E00314>
- [9] Özbek, N. A.; Özbek, O.; Kara, F.; Statistical Analysis of the Effect of the Cutting Tool Coating Type on Sustainable Machining Parameters. *J Mater Eng Perform.*, 2021, 30, 7783–7795. <https://doi.org/10.1007/s11665-021-06066-8>
- [10] Guillaume, C. E.; Invar and Elinvar. *Nobel Lect Phys.*, 1967, 444–473.
- [11] Davis, J. R.; Alloying: Understanding the Basics. ASM International: Materials Park, 2001, OH.
- [12] Rosenberg, S. J.; Nickel and its alloys, National Bureau of Standards Monograph. Institute for Materials Research, 1968, Washington, DC.
- [13] Nickel-Iron Alloys. <https://www.specialmetals.com/assets/smc/documents/alloys/nilo-nilomag/nilo-and-nilomag-alloys.pdf>
- [14] Wei, K.; Yang, Q.; Ling, B.; et al.; Mechanical properties of Invar 36 alloy additively manufactured by selective laser melting. *Mater Sci Eng A*, 2020, 772, 138799. <https://doi.org/10.1016/J.MSEA.2019.138799>
- [15] Nagayama, T.; Yamamoto, T.; Nakamura, T.; Electrodeposition of Invar Fe-Ni Alloy/SiC Particle Composite. *ECS Trans.*, 2017, 75, 69–77. <https://doi.org/10.1149/07537.0069ecst>
- [16] Nagayama, T.; Yamamoto, T.; Nakamura, T.; Thermal expansions and mechanical properties of electrodeposited Fe–Ni alloys in the Invar composition range. *Electrochim Acta*, 2016, 205, 178–187. <https://doi.org/10.1016/J.ELECTACTA.2016.04.089>
- [17] Ratnayake, D.; Derakhshani, M.; Berfield, T. A.; Walsh, K. M.; Bistability study of buckled MEMS diaphragms. *J Phys Commun* 2020, 4, 105008. <https://doi.org/10.1088/2399-6528/abbe5e>
- [18] Corbacho, J. L.; Suárez, J. C.; Molleda, F.; Welding of invar Fe-36Ni alloy for tooling of composite materials. *Weld Int.*, 1998, 12, 314

- 966–971.
<https://doi.org/10.1080/09507119809448543>
- [19] Hidalgo, J.; Jiménez-Morales, A.; Barriere, T.; et al.; Mechanical and functional properties of Invar alloy for μ -MIM. *Powder Metall.*, 2014, 57, 127–136.
<https://doi.org/10.1179/1743290113Y.0000000081>
- [20] Ezugwu, E. O.; Wang, Z. M.; Machado, A. R.; The machinability of nickel-based alloys: a review. *J Mater Process Technol.*, 1999, 86, 1–16. [https://doi.org/10.1016/S0924-0136\(98\)00314-8](https://doi.org/10.1016/S0924-0136(98)00314-8)
- [21] Asgari, H.; Salarian, M.; Ma, H.; et al.; On thermal expansion behavior of invar alloy fabricated by modulated laser powder bed fusion. *Mater Des.*, 2018, 160, 895–905.
<https://doi.org/10.1016/J.MATDES.2018.10.025>
- [22] Kivak, T.; Optimization of surface roughness and flank wear using the Taguchi method in milling of Hadfield steel with PVD and CVD coated inserts. *Measurement*, 2014, 50, 19–28.
<https://doi.org/10.1016/J.MEASUREMENT.2013.12.017>
- [23] Ezugwu, E. O.; Okeke, C. I.; Behavior of Coated Carbide Tools in High Speed Machining of a Nickel Base Alloy. *Tribol Trans.*, 2002, 45, 122–126.
<https://doi.org/10.1080/10402000208982530>
- [24] Ezugwu, E. O.; Wang, Z. M.; Okeke, C. I.; Tool Life and Surface Integrity When Machining Inconel 718 With PVD- and CVD-Coated Tools. *Tribol Trans.*, 1999, 42, 353–360.
<https://doi.org/10.1080/10402009908982228>
- [25] Jawaid, A.; Koksai, S.; Sharif, S.; Wear Behavior of PVD and CVD Coated Carbide Tools when Face Milling Inconel 718. *Tribol Trans.*, 2000, 43, 325–331.
<https://doi.org/10.1080/10402000008982347>
- [26] García, J.; Collado Ciprés, V.; Blomqvist, A.; Kaplan, B.; Cemented carbide microstructures: a review. *Int J Refract Met Hard Mater.*, 2019, 80, 40–68.
<https://doi.org/10.1016/J.IJRMHM.2018.12.004>
- [27] Tool-life testing with single-point turning tools. ISO 3685, 1993.
- [28] Ciftci, I.; Machining of austenitic stainless steels using CVD multi-layer coated cemented carbide tools. *Tribol Int.*, 2006, 39, 565–569.
<https://doi.org/10.1016/j.triboint.2005.05.005>
- [29] Korkut, I.; Donertas, M. A.; The influence of feed rate and cutting speed on the cutting forces, surface roughness and tool–chip contact length during face milling. *Mater Des.*, 2007, 28, 308–312.
<https://doi.org/10.1016/J.MATDES.2005.06.002>
- [30] Bagherzadeh, A.; Budak, E.; Investigation of machinability in turning of difficult-to-cut materials using a new cryogenic cooling approach. *Tribol Int.*, 2018, 119, 510–520.
<https://doi.org/10.1016/J.TRIBOINT.2017.11.033>
- [31] Saleem, M. Q.; Mumtaz, S.; Face milling of Inconel 625 via wiper inserts: Evaluation of tool life and workpiece surface integrity. *J Manuf Process*, 2020, 56, 322–336.
<https://doi.org/https://doi.org/10.1016/j.jmapro.2020.04.011>
- [32] Kaladhar, M.; Venkata Subbaiah, K.; Srinivasa Rao, C.; Narayana Rao, K.; Process parameters optimisation and coatings influence on the surface quality during turning of AISI 202 austenitic stainless steel. *Int J Mach Mach Mater.*, 2012, 11, 371–384.
<https://doi.org/10.1504/IJMMM.2012.047832>
- [33] Kara, F.; Öztürk, B.; Comparison and optimization of PVD and CVD method on surface roughness and flank wear in hard-machining of DIN 1.2738 mold steel. *Sens Rev.*, 2019, 39, 24–33.
<https://doi.org/10.1108/SR-12-2017-0266>
- [34] Ginting, A.; Skein, R.; Cuaca, D.; et al.; The characteristics of CVD- and PVD-coated carbide tools in hard turning of AISI 4340. *Measurement*, 2018, 129, 548–557.
<https://doi.org/10.1016/J.MEASUREMENT.2018.07.072>
- [35] Özbek, O.; Saruhan, H.; The effect of vibration and cutting zone temperature on surface roughness and tool wear in eco-friendly MQL turning of AISI D2. *J Mater*

Res Technol., 2020, 9, 2762–2772.
<https://doi.org/10.1016/J.JMRT.2020.01.010>

- [36] Sun, X.; Li, J.; Cameron, D.; Zhou, A.; Field monitoring and assessment of the impact of a large eucalypt on soil desiccation. *Acta Geotech.* 2021,
<https://doi.org/10.1007/s11440-021-01308-4>
- [37] Cetin, M. H.; Ozcelik, B.; Kuram, E.; Demirbas, E.; Evaluation of vegetable based cutting fluids with extreme pressure and cutting parameters in turning of AISI 304L by Taguchi method. *J Clean Prod.*, 2011, 19, 2049–2056.
<https://doi.org/10.1016/J.JCLEPRO.2011.07.013>
- [38] Özlü, B.; Experimental and statistical investigation of the effects of cutting parameters on kerf quality and surface roughness in laser cutting of Al 5083 alloy. *Surf Rev Lett.*, 2021 28, 2150093.
<https://doi.org/10.1142/S0218625X21500931>